Short Communication

Institution of MECHANICAL ENGINEERS
Journal of ENGINEERING MANUFACTURE

Proc IMechE Part B:
J Engineering Manufacture
2016, Vol. 230(3) 593–600

DOI: 10.1177/0954405414551107
pib.sagepub.com
SAGE

Static pointing error analysis of electro-optical detection systems

Qijian Tang[1,2], Xiangjun Wang[1] and Qingping Yang[2]

Abstract

Electro-optical detection systems have been widely utilized in many applications. The pointing accuracy is often seriously affected by static geometric errors. This article analyses the contributions of integrant geometric error sources by means of quaternions, and a parametric model is hence established. As to nonlinear errors, this article further proposes a semi-parametric model that is based on least squares collocation method. Test results demonstrate that both models can improve the pointing accuracy effectively, with latter offering better performance. The estimation variances in azimuth and elevation validation test have been reduced to 0.0014(°)^2 and 0.0009 (°)^2 from 0.0258(°)^2 and 0.0017(°)^2, respectively.

Keywords

Pointing error, Quaternion, semi-parametric model, error compensation, electro-optical detection system

Date received: 24 June 2014; accepted: 20 August 2014

Introduction

Inertially stabilized platforms (ISPs) have been widely used to maintain its sensor's orientation in an accurate direction in many applications, such as vehicles, ships, aircrafts and spacecraft.[1–4] Electro-optical detection systems (EODSs) including optical imaging sensors and ISPs are utilized to collect targets' location information, which is of great significance in scientific, military and commercial applications.[2,5] In the manufacturing and assembly processes, it is inevitable to introduce errors such as misalignment error, nonperpendicularity and initialization error, which can result in the static pointing error.[6,7] As a key technical parameter of the front measuring module, static pointing accuracy significantly affects the target tracking and location. Therefore, it is necessary to model and calibrate these errors to improve the pointing accuracy.[8] At present, there are various approaches to establish the error model, such as Debye–Hückel (D–H) equation[4,9] and coordinate transformation (rotation matrix).[10] Since quaternions can visually represent a rotation,[11] this article employs quaternions to analyse integrant errors of EODS for the first time. There are still nonlinear errors that cannot be compensated for by parametric model, such as mechanical deformation and environment factors. It further improves the pointing accuracy by means of semi-parameter model.

Pointing error modelling

The EODS is a servo-controlled system including inner and outer gimbals, which rotate around azimuth and elevation axes, as shown in Figure 1, with the imaging sensor fixed on the inner gimbal. The rotated angles are defined as azimuth and elevation, respectively. Rate gyroscopes are utilized to measure the rotation speed and sense the platform vibration to attenuate the disturbance to the line of sight (LOS).[2–5] Proper control algorithm will increase dynamic pointing accuracy in inertial space and hold LOS stationary to obtain clear target images. Position sensors such as optical-electricity encoders or rotary transformers are utilized to obtain the rotation angle, and the spatial pointing direction of LOS can hence be calculated.[1] This article focuses on the geometric errors of EODS without considering dynamic control error.

[1]MOEMS Education Ministry Key Laboratory, Tianjin University, Tianjin, China
[2]School of Engineering and Design, Brunel University, Middlesex, UK

Corresponding author:
Xiangjun Wang, MOEMS Education Ministry Key Laboratory, Tianjin University, Tianjin 300072, China.
Email: xdocuxjw@vip.163.com

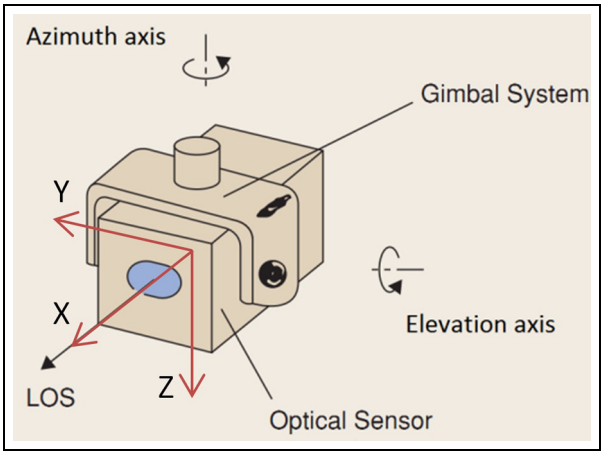

Figure 1. Two-axial gimbal system.
LOS: line of sight.

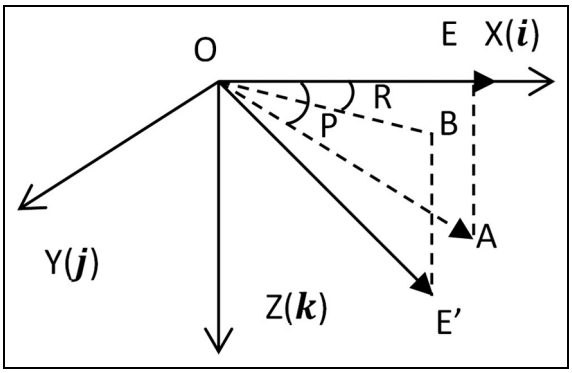

Figure 2. Schematic diagram of rotation angles.

Ideal pointing direction

To facilitate the analysis, the coordinate system is established as shown in Figure 1. At the 0 positions, azimuth axis is the OZ-axis, elevation axis is the OY-axis and the ideal LOS is coincident with OX-axis, which are in accord with the right-hand coordinate system. Furthermore, the rotation angles are defined as shown in Figure 2. The LOS OE rotates R and P around the azimuth (OZ)- and elevation (OY)-axes, respectively, to OE'.

Invented by W.R. Hamilton, quaternions can be used to speed up calculations involving rotations. A quaternion is represented by just four scalars, in contrast to a 3×3 rotation matrix that has nine scalar entries.[12,13] A unit quaternion is used to denote a rotation.[11,14] Assume the rotation around the elevation axis is first analysed, then around the azimuth axis. The rotation quaternions are shown in equations (1) and (2), where the counter-clockwise is positive

$$Q_y = \cos\frac{P}{2} + \boldsymbol{j}\sin\frac{P}{2} \tag{1}$$

$$Q_z = \cos\frac{R}{2} + \boldsymbol{k}\sin\frac{R}{2} \tag{2}$$

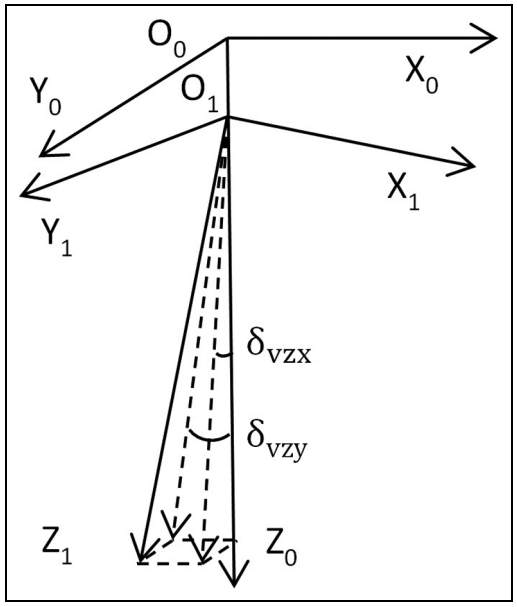

Figure 3. Azimuth axis nonperpendicularity.

The original vector can be described as $OE = \boldsymbol{i}$. Therefore, the ideal pointing direction vector is

$$OE' = (Q_z Q_y)OE(Q_z Q_y)^* = \boldsymbol{i}\cos R\cos P + \boldsymbol{j}\sin R\cos P - \boldsymbol{k}\sin P \tag{3}$$

Integrant error analysis

Nonperpendicularity. Ideally, the rotation axes of EODS are perpendicular to each other. However, axis nonperpendicularity may result from the assembling process, with misalignments among azimuth axis, elevation axis and the carrier. For instance, the EODS is fixed on an unmanned aerial vehicle (UAV); if the azimuth axis tilts from the vehicle, although the measurement of EODS is accurate, it will introduce errors to the target location in the whole system. The inclined angular components around OX- and OY-axes are δ_{vzx} and δ_{vzy}, as shown in Figure 3, where $O_0X_0Y_0Z_0$ is the coordinate system of the vehicle and $O_1X_1Y_1Z_1$ is the coordinate system of EODS.

Take the bias around OX-axis as an example; the process is equivalent to rotating R and P first, then it continues to rotate a small angle δ_{vzx} around OX-axis. The quaternion is

$$Q_{1zx} = Q_\delta Q_z Q_y = \left(\cos\frac{\delta_{vzx}}{2} + \boldsymbol{i}\sin\frac{\delta_{vzx}}{2}\right)\left(\cos\frac{R}{2} + \boldsymbol{k}\sin\frac{R}{2}\right)\left(\cos\frac{P}{2} + \boldsymbol{j}\sin\frac{P}{2}\right) \tag{4}$$

The actual pointing direction is defined as OE'', and the inclined angles with OE' are ΔR and ΔP in terms of azimuth and elevation, respectively

$$OE'' = Q_{1zx}OEQ*_{1zx} = \boldsymbol{i}\cos R\cos P + \boldsymbol{j}(\sin R\cos P\cos\delta_{vzx} + \sin P\sin\delta_{vzx}) + \boldsymbol{k}(\sin R\cos P\sin\delta_{vzx} - \sin P\cos\delta_{vzx}) \tag{5}$$

As ΔR and ΔP are very small, it can be assumed that $\sin \Delta R = \Delta R$, $\cos \Delta R = 1$ and $\Delta R \times \Delta R = 0$, which are also applied to ΔP. Combining equations (3) and (5), the following can be obtained

$$\begin{cases} \dfrac{\sin(R+\Delta R)\cos(P+\Delta P)}{\cos(R+\Delta R)\cos(P+\Delta P)} = \dfrac{\sin R \cos P \cos \delta_{vzx} + \sin P \sin \delta_{vzx}}{\cos R \cos P} \\ \sin(P+\Delta P) = -\sin R \cos P \sin \delta_{vzx} + \sin P \cos \delta_{vzx} \end{cases} \quad (6)$$

Then

$$\begin{cases} \Delta R \approx \delta_{vzx} \cos R \tan P \\ \Delta P \approx -\delta_{vzx} \sin R \end{cases} \quad (7)$$

Other nonperpendicularity errors can also be computed in the same way.

Optical axis misalignment and initialization error. In the assembly process, it is also difficult to keep the LOS aligned with OX-axis, which will result in the LOS rotating around OY- and OZ-axes. The inclined angular components are defined as δ_{vxy} and δ_{vxz}, respectively, as shown in Figure 4, where $O_1X_1Y_1Z_1$ is the coordinate system of EODS and O_1X' is the initial LOS. It is obvious that the optical axis misalignment will definitely introduce measurement error. The computation is similar to section "Nonperpendicularity." Meanwhile, high-precision locations are based on the accurate initial position. The initialization error will directly affect the LOS accuracy. The method above also applies to initialization error analysis.

Encoder scale error. Adopting the encoder scale error analysis of telescopes in Luck,[15] the error is

$$\begin{cases} R = \frac{Q_1 R}{2\pi} \\ \Delta P = \frac{Q_2 R}{2\pi} \end{cases} \quad (8)$$

where Q_1 and Q_2 are the coefficients.

Rotating shaft error. Bearings define the rotating shaft position and allow the axes to run freely. Wobble and runout in a bearing cause the instantaneous axis of rotation to change and directly result in pointing error.[16] The rotating shaft error is shown in Figure 5, where Δs is the axial runout, Δc is the radical runout and ρ is the slant angle.[17]

Rotating shaft error will cause the encoder eccentricity, resulting in the indication error. As shown in Figure 6, the dashed line denotes the original position, and the solid line denotes the tilted encoder disc position. L is the distance from the intersection of shaft axis before and after tilting to the encoder centre, r is the encoder's radius and $(\rho L + \Delta c)$ is the eccentric distance. θ is the actual value and θ' is the ideal value.

It can be shown that

$$\Delta\theta \approx -\sin\theta \times \rho Q \quad (9)$$

where $Q = L/\sqrt{2\rho L r + r^2}$

As to the azimuth and elevation axes, the slant angles are assumed as ρ_{rzy}, ρ_{rzx}, ρ_{ryz} and ρ_{ryx}. For the azimuth axis, $\Delta P = 0$; for the elevation axis, $\Delta R = 0$, and the rest of errors could be calculated through equation (9).

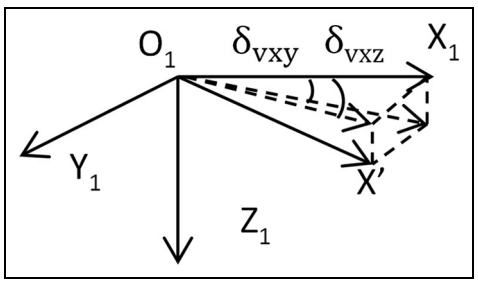

Figure 4. Optical axis misalignment.

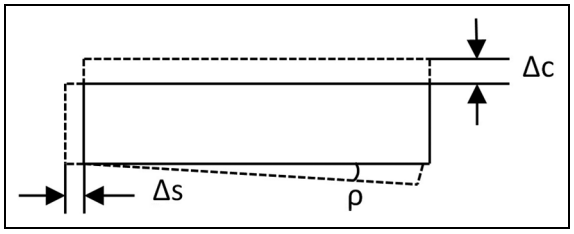

Figure 5. Rotating shaft error.

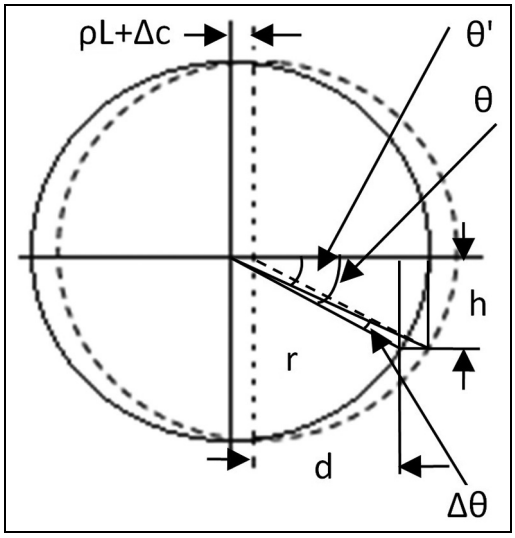

Figure 6. Encoder eccentricity.

Table 1. Integrant error summary.

Integrant error	Notion	Contribution to ΔR	Contribution to ΔP
Nonperpendicularity (azimuth, OX)	δ_{vzx}	$\delta_{vzx}\cos R\tan P$	$-\delta_{vzx}\sin R$
Nonperpendicularity (azimuth, OY)	δ_{vzy}	$\delta_{vzy}\sin R\tan P$	$\delta_{vzy}\cos R$
Nonperpendicularity (elevation, OX)	δ_{vyx}	$\delta_{vyx}\tan P$	0
Nonperpendicularity (elevation, OZ)	δ_{vyz}	δ_{vyz}	0
Optical axis misalignment (OY)	δ_{vxy}	0	δ_{vxy}
Optical axis misalignment (OZ)	δ_{vxz}	$\delta_{vxz}\sec P$	0
Initialization error (elevation)	η_y	0	η_y
Initialization error (azimuth)	η_z	η_z	0
Encoder scale error (elevation)	$Q_1P/2\pi$	0	$Q_1P/2\pi$
Encoder scale error (azimuth)	$Q_2R/2\pi$	$Q_2R/2\pi$	0
Rotating shaft error (elevation, OX)	ρ_{ryx}	0	$-Q_3\rho_{ryx}\cos P$
Rotating shaft error (elevation, OZ)	ρ_{ryz}	0	$-Q_4\rho_{ryz}\sin P$
Rotating shaft error (azimuth, OX)	ρ_{rzx}	$-Q_5\rho_{rzx}\cos R$	0
Rotating shaft error (azimuth, OY)	ρ_{rzy}	$-Q_6\rho_{rzy}\sin R$	0

$Q_1 - Q_6$ are the coefficients.

Integrant error summary

According to the above description, the errors are presented in Table 1.

Adding all the contributions, the final integrant error model is hence obtained

$$\begin{cases} \Delta R = \delta_{vyx}\tan P + \delta_{vyz} + \delta_{vzx}\cos R\tan P + \delta_{vzy}\sin R\tan P + \delta_{vxz}\sec P - Q_5\rho_{rzx}\cos R - Q_6\rho_{rzy}\sin R \\ \quad + \eta_z + \dfrac{Q_2R}{2\pi} = C_1 + C_2R + C_3\sin R + C_4\cos R + C_5\sec P + C_6\tan P + C_7\cos R\tan P + C_8\sin R\tan P \\ \Delta P = -\delta_{vzx}\sin R + \delta_{vzy}\cos R + \delta_{vxy} - Q_3\rho_{ryx}\cos P - Q_4\rho_{ryz}\sin P + \eta_y + \dfrac{Q_1P}{2\pi} \\ \quad = C_9 + C_{10}P + C_{11}\sin P + C_{12}\cos P + C_{13}\sin R + C_{14}\cos R \end{cases} \tag{10}$$

where $C_1 - C_{14}$ are the coefficients.

Semi-parametric model

The integrant error model presented in equation (10) is based on geometric errors, which is a parametric model. There are still nonlinear errors that are not considered, such as the environment factors including temperature, atmosphere, gravity, wind and vibration.[4,5] To improve the pointing accuracy, it is necessary to compensate for these nonlinear errors. Since a semi-parametric model contains both parametric and nonparametric components, it provides a convenient way to analyse nonlinearities and has been widely used.[18–20]

Least squares collocation

As an estimation method for semi-parametric model, least square collocation has also been widely used. The model can be written as[4,18]

$$\delta = GX + h + \varepsilon \tag{11}$$

where δ is the pointing error observations, which is expected to be 0; X is the input vector and G is the coefficient vector. δ, G and X are equivalent to parameters in the parametric model presented in equation (10); ε is the process noise and the variance $D_\varepsilon = \sigma^2 I$. h denotes the systemic error, which is the nonparametric component as it is difficult to express with limited parametric model.

According to equation (11), the estimated error of the model is shown as follows

$$V = G\hat{X} + \hat{h} - \delta \tag{12}$$

where V is the residual and $\hat{X}$ and $\hat{h}$ are the estimates of X and h.

To identify the optimal estimate of equation (12), a commonly used solution is adding a penalty term to standard least squares as shown in equation (13), and relevant derivation is also presented in Hong et al.,[4] Sun and Wu[18] and Pan and Sun[21]

$$V^TV + \alpha\hat{h}^TR_f\hat{h} = min \tag{13}$$

where α is the smoothing factor, which is used for the balance between V and X; R_f is the regular matrix, representing certain function of the nonparametric parts.

According to Lagrange multiplier rules, the Lagrange function Φ is constructed as

$$\Phi = V^TV + \alpha\hat{h}^TR_f\hat{h} + 2K(G\hat{X} + \hat{h} - \delta - V) \tag{14}$$

where K is the Lagrange multiplier. Let partial derivatives of V, $\hat{X}$ and $\hat{h}$ in equation (14) be 0, then

$$\begin{cases} K = V \\ K = -\alpha R_f\hat{h} \\ G^TK = 0 \end{cases} \tag{15}$$

After the elimination of K in equation (15), combined with equation (12), the below can be obtained

$$G^TG\hat{X} + G^T\hat{h} - G^T\delta = 0 \tag{16}$$

Table 2. Compensation comparison of parametric model and semi-parametric model.

	Original	Parametric model	Semi-parametric model
Mean (°) (azimuth)	−0.1674	−6.1238e − 16	5.6585e − 17
Variance ((°)^2) (azimuth)	0.0492	0.0039	3.4308e − 6
Mean (°) (elevation)	0.0454	1.2512e − 16	3.3654e − 16
Variance ((°)^2) (elevation)	0.0065	0.0012	1.8077e − 8

From equations (12) and (15), the below can also be obtained

$$G\hat{X} + \hat{h} - \delta + \alpha R_f \hat{h} = 0 \tag{17}$$

Combining equations (16) and (17), the estimate of X and h are finally obtained

$$\begin{cases} \hat{h} = M^{-1}(I - G(G^TG)^{-1}G^T)\delta \\ \hat{X} = (G^TG)^{-1}G^T(\delta - \hat{h}) \end{cases} \tag{18}$$

where $M = I + \alpha R_f - G(G^TG)^{-1}G^T$

Selection of α and R_f

As the smoothing factor, α is critical for the balance between the residual and the signal. Cross-validation method commonly used in nonparametric estimation is also suitable for semi-parametric estimation. It works by withholding a single data point at a time while using the rest of the data to predict the withheld response. The value of α with the smallest cross-validated squared error is then taken to be the best one.[21,22]

There are many approaches to choosing the regular matrix R_f; in this article, it was chosen according to the distance of each point. The data points are $(x_1, y_1), (x_2, y_2), \ldots, (x_n, y_n)$

Thus

$$R_{fij} = \sqrt{(x_i - x_j)^2 + (y_i - y_j)^2} \quad (1 \leqslant i, j \leqslant n) \tag{19}$$

Test results

The data acquisition system mainly contains a high-precision triaxial turntable, an autocollimator and the EODS. The reflection mirror is fixed on the inner gimbal of EODS. The EODS is fixed on the middle axis of the turntable. The angular range is −20° to 20° for azimuth and −20° to 10° for elevation, with the test apparatus shown in Figure 7. The turntable provides precision rotatory angles, the EODS rotates in the opposite direction and the autocollimator presents the pointing errors.

Once the systemic errors of the calibration system are known, the compensation results by parametric model presented in equation (10) and semi-parametric model presented in equation (12) are given out in Figure 8 and Table 2 in terms of azimuth and elevation.

The results demonstrated that the pointing error is effectively compensated. Using the parametric model,

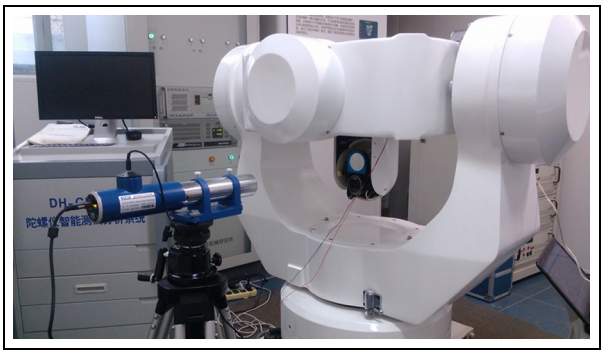

Figure 7. EODS calibration.

the variance in azimuth error has decreased by an order of magnitude, and the elevation error has decreased to 0.0012(°)^2 from 0.0065(°)^2. In contrast, the semi-parametric model has achieved more significant reductions. From the fitting coefficients, it can be seen that the nonperpendicularity both from azimuth and elevation is the main error source. Meanwhile, to verify the effectiveness of established models still further, another set of data points are acquired. The estimation results by both parametric and semi-parametric model are shown in Table 3 and Figure 9.

According to the estimation results, for the azimuth, the variance has decreased from 0.0258(°)^2 to 0.0042(°)^2 and 0.0014(°)^2 by parametric and semi-parametric models, respectively. The mean value reduction is at least by an order of magnitude. For the elevation, the variance has reduced to 0.0016(°)^2 and 0.0009(°)^2 from the original 0.0017(°)^2. Especially, with the semi-parametric model estimated, the absolute value of the pointing residual of azimuth is less than 0.06° except the last point which may have a gross error. All these estimation results indicate that both parametric and semi-parametric models developed in this article can improve the pointing accuracy effectively, and the latter presents better superiority.

Conclusion

With regard to the pointing error of EODS, this article has employed quaternions to analyse contributions from a set of integrant geometric error sources including nonperpendicularity, optical axis misalignment, initialization error, encoder scale error and rotating shaft error. It has hence established the parametric

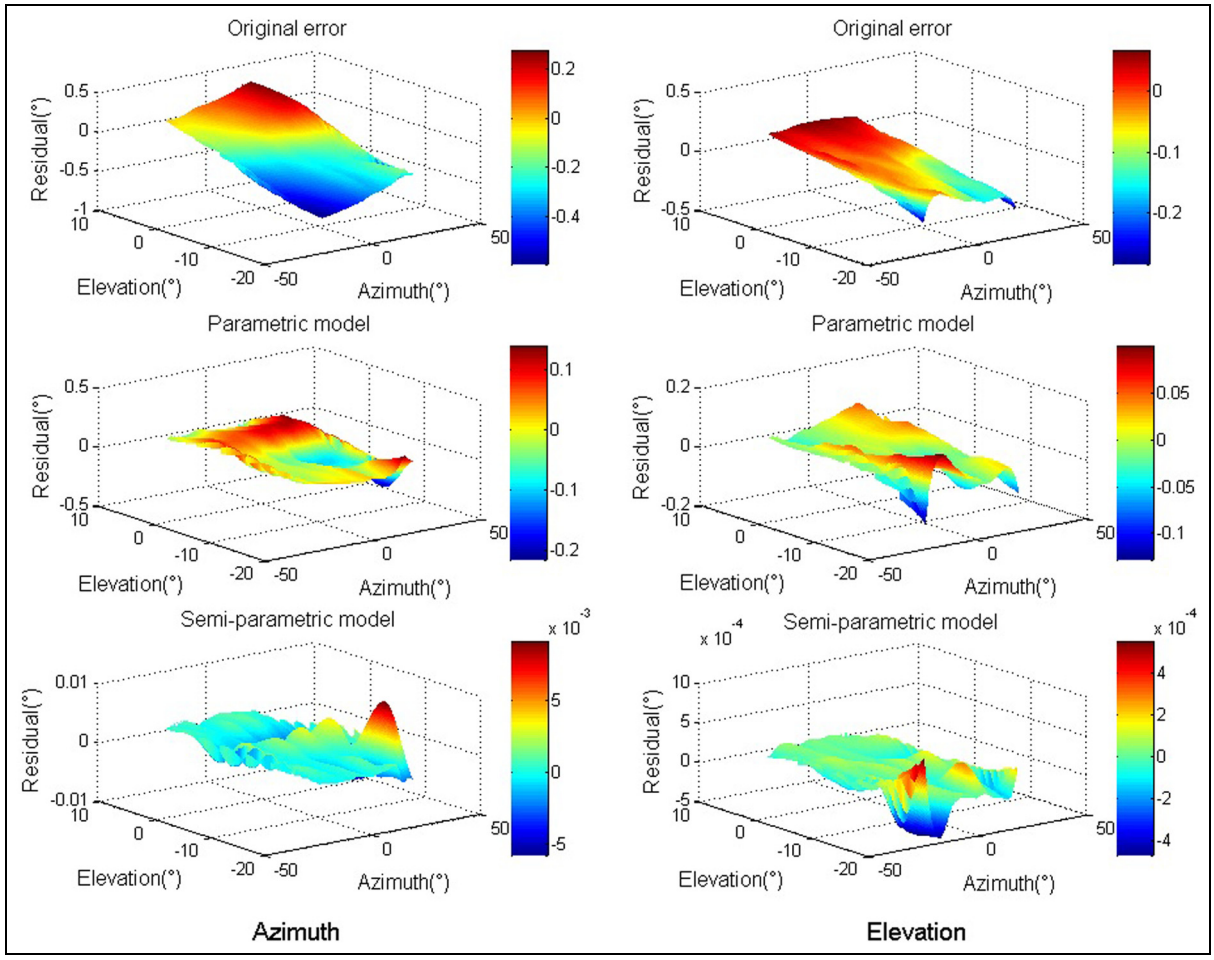

Figure 8. Comparison of compensation results.

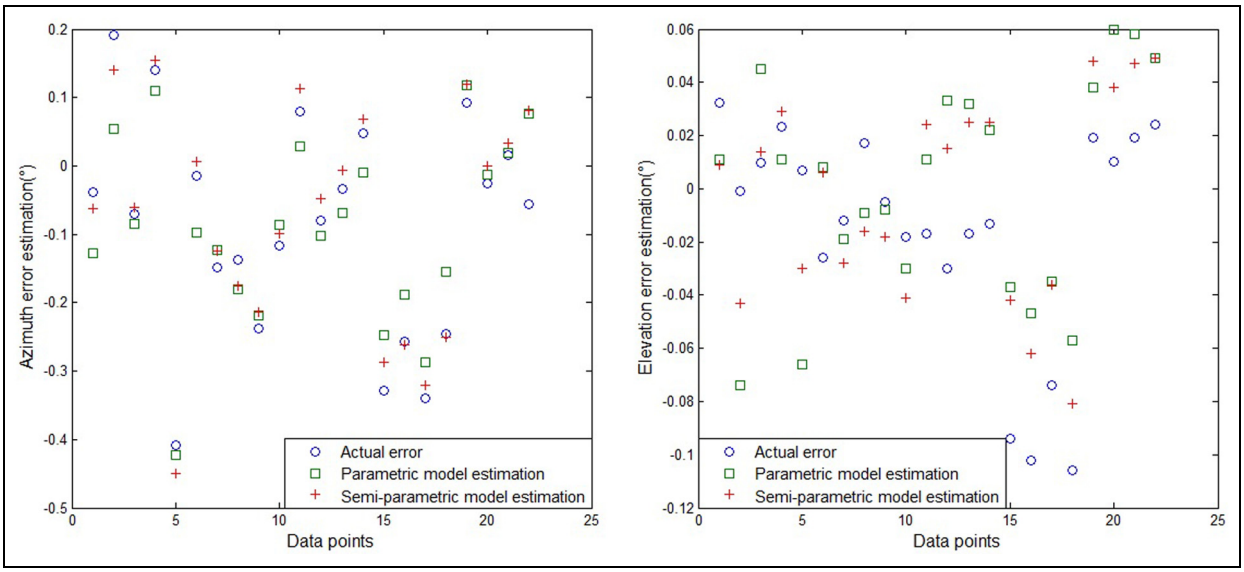

Figure 9. Estimation results.

model of pointing error. The fitting coefficient values indicate that nonperpendicularity is the main error source. Test results have shown that the parametric model can compensate for the error effectively, with the variance reduced from $0.0258(°)^2$ to $0.0042(°)^2$ for the azimuth. In order to compensate for the nonlinear

Table 3. Model verification.

Test position (°)	Pointing error (°)		Test position (°)	Pointing error (°)		
	Parametric model	Semi-parametric model	Actual measurement		Parametric model	Semi-parametric model	Actual measurement
(3, 0)	(−0.127, 0.011)	(−0.063, 0.009)	(−0.038, 0.032)	(7, −3)	(−0.102, 0.033)	(−0.048, 0.015)	(−0.080, −0.030)
(−21, 0)	(0.054, −0.074)	(0.140, −0.043)	(0.191, −0.001)	(3, −3)	(−0.068, 0.032)	(−0.006, 0.025)	(−0.034, −0.017)
(11, −5)	(−0.085, 0.045)	(−0.060, 0.014)	(−0.070, 0.010)	(−3, −3)	(−0.010, 0.022)	(0.068, 0.025)	(0.048, −0.013)
(−11, −5)	(0.110, 0.011)	(0.155, 0.029)	(0.140, 0.023)	(3, 7)	(−0.247, −0.037)	(−0.287, −0.042)	(−0.328, −0.094)
(17, 10)	(−0.423, −0.066)	(−0.450, −0.030)	(−0.408, 0.007)	(−3, 7)	(−0.188, −0.047)	(−0.261, −0.062)	(−0.257, −0.102)
(0, 0)	(−0.098, 0.008)	(0.006, 0.006)	(−0.014, −0.026)	(7, 7)	(−0.287, −0.035)	(−0.321, −0.036)	(−0.339, −0.074)
(−3, 3)	(−0.123, −0.019)	(−0.125, −0.028)	(−0.149, −0.012)	(−7, 7)	(−0.154, −0.057)	(−0.251, −0.081)	(−0.246, −0.106)
(3, 3)	(−0.181, −0.009)	(−0.175, −0.016)	(−0.138, 0.017)	(−7, −7)	(0.118, 0.038)	(0.119, 0.048)	(0.093, 0.019)
(7, 3)	(−0.219, −0.008)	(−0.214, −0.018)	(−0.237, −0.005)	(7, −7)	(−0.013, 0.060)	(0.000, 0.038)	(−0.025, 0.010)
(−7, 3)	(−0.087, −0.030)	(−0.099, −0.041)	(−0.116, −0.018)	(3, −7)	(0.019, 0.058)	(0.033, 0.047)	(0.016, 0.019)
(−7, −3)	(0.029, 0.011)	(0.113, 0.024)	(0.079, −0.017)	(−3, −7)	(0.077, 0.049)	(0.081, 0.049)	(−0.056, 0.024)

errors except geometric errors, it has further developed the semi-parametric pointing error model, and the variances in azimuth and elevation have declined to $0.0014(^\circ)^2$ and $0.0009(^\circ)^2$ from $0.0258(^\circ)^2$ and $0.0017(^\circ)^2$, respectively, which demonstrates that the semi-parametric model is more effective and powerful.

Declaration of Conflicting Interests

The author(s) declared no potential conflicts of interest with respect to the research, authorship, and/or publication of this article.

Funding

The author(s) disclosed receipt of the following financial support for the research, authorship, and/or publication of this article: The work was supported by Support Program of National Ministry of Education of China (No. 625010110) and National Natural Science Foundation of China (No. 61179043). It was also supported by China Scholarship Council.

References

1. Hilkert JM. Inertially stabilized platform technology. *IEEE Contr Syst Mag* 2008; 28: 26–46.
2. Michael KM. Inertially stabilized platforms for optical imaging systems. *IEEE Contr Syst Mag* 2008; 28: 47–64.
3. Ekstrand B. Equations of motion for a two-axes gimbal system. *IEEE T Aero Elec Syst* 2001; 37: 1083–1091.
4. Hong HJ, Zhou XY, Zhang ZY, et al. Modelling and calibration of pointing errors using a semi-parametric regression method with applications in inertially stabilized platforms. *Proc IMechE, Part B: J Engineering Manufacture*. Epub ahead of print 16 August 2013. DOI: 10.1177/0954405413475559.
5. Zhang ZY, Zhou XY and Fan DP. Analysis, modelling and correction of pointing errors for electro-optical detection systems. *Acta Aeronautica Astronautica Sinica* 2011; 32: 2042–2054.
6. Wang JQ, Jin G and Yan CX. Orientation error analysis of airborne opto-electric tracking and measuring device. *Optic Precis Eng* 2005; 13: 105–116.
7. Li Y and Fan DP. Development of pointing error and sensitivity analysis of opto-electrical stabilization mechanism. *J National Univ Defense Tech* 2008; 30: 104–109.
8. Rue AK. Calibration of precision gimballed pointing systems. *IEEE T Aero Elec Syst* 1970; AES-6: 697–706.
9. Sladek J, Ostrowska K and Gaska A. Modelling and identification of errors of coordinate measuring arms with the use of a metrological model. *Measurement* 2013; 46: 667–679.
10. Meeks ML, Ball JA and Hull AB. The pointing calibration of the Haystack antenna. *IEEE T Antenn Propag* 1968; 16: 746–751.
11. Goldman R. Understanding quaternions. *Graph Model* 2011; 73: 21–49.
12. Meister L. Mathematical modelling in geodesy based on quaternion algebra. *Phys Chem Earth A* 2000; 25: 661–665.

13. Meister L and Schaeben H. A concise quaternion geometry of rotations. *Math Meth Appl Sci* 2005; 28: 101–126.
14. Zhao Y, Zhang XF and Shi HL. Pointing error analysis of a radio telescope using quaternion. *Mech Sci Tech Aerospace Eng* 2009; 28: 1359–1369.
15. Luck JM. Mount model stability. Report, EOS Space Systems Pty Ltd, Canberra, ACT, Australia, May, 2004.
16. Meeks RL. *Improving telescope mechanical error estimates using pointing data*. PhD Thesis, Colorado State University, Fort Collins, CO, 2003, pp.30–33.
17. Li Y. *A study on error modelling and evaluation of electro-optical stabilization tracking equipment*. PhD Thesis, National University of Defense Technology, Changsha, China, 2007, pp.61–62.
18. Sun HY and Wu Y. Semiparametric regression and model refining. *Geo Spatial Inform Sci* 2002; 5: 10–13.
19. Shi P and Tsai CL. Semiparametric regression model selections. *J Stat Plan Infer* 1999; 77: 119–139.
20. Zhang WY, Fan JQ and Sun Y. A semiparametric model for cluster data. *Ann Stat* 2009; 37: 2377–2408.
21. Pan X and Sun HY. Parameter estimation of least squares collocation. *Eng Survey Map* 2004; 13: 5–11.
22. Carmack PS, Spence JS and Schucany WR. Generalised correlated cross-validation. *J Nonparametr Stat* 2012; 24: 269–282.

Appendix 1

Notation

$C_1 - C_{14}$	coefficients of parametric model
D_ε	variance in process noise, $D_\varepsilon = \sigma^2 I$
G	coefficient vector of pointing error model
h	systemic segment in pointing error
$\hat{h}$	the estimate of h
i, j, k	basis of quaternions
K	Lagrange multiplier
L	distance from the intersection of shaft axis before and after tilting to the encoder centre
M	intermediate matrix, $M = I + \alpha R_f - G(G^T G)^{-1} G^T$
OE	initial pointing direction
OE'	ideal rotated pointing direction
OE''	actual pointing direction
	$O_0X_0Y_0Z_0$ coordinate system of the vehicle
	$O_1X_1Y_1Z_1$ coordinate system of EODS
P	rotated azimuth angle
Q	coefficient of encoder eccentricity error
$Q_1 - Q_6$	coefficients, $Q_1 - Q_2$ are coefficients of encoder scale error, $Q_3 - Q_6$ are coefficients of encoder eccentricity error
Q_y	rotation quaternion of elevation
Q_z	rotation quaternion of azimuth
Q_{1zx}	equivalent quaternion of azimuth axis nonperpendicularity around X-axis
Q_δ	rotation quaternion of small angle δ_{vzx} around X-axis
r	encoder's radius
R	rotated elevation angle
R_f	regular matrix, representing certain function of the nonparametric parts
R_{fij}	element of R_f, $R_{fij} = \sqrt{(x_i - x_j)^2 + (y_i - y_j)^2}$ $(1 \leqslant i, j \leqslant n)$
T	transposition of matrix
V	residual of model estimation
x_i	azimuth of test positions $(1 \leqslant i \leqslant n)$
X	input vector of pointing error model
$\hat{X}$	estimate of X
y_i	elevation of test positions $(1 \leqslant i \leqslant n)$
α	smoothing factor, used for the balance between V and X
Δc	radical runout of shaft
ΔP	pointing error of azimuth
ΔR	pointing error of elevation
Δs	axial runout of shaft
$\Delta\theta$	encoder eccentricity error
δ	pointing error observations
δ_{vxy}	optical axis misalignment around Y-axis
δ_{vxz}	optical axis misalignment around Z-axis
δ_{vyx}	elevation axis nonperpendicularity around OX-axis
δ_{vyz}	elevation axis nonperpendicularity around OZ-axis
δ_{vzx}	azimuth axis nonperpendicularity around OX-axis
δ_{vzy}	azimuth axis nonperpendicularity around OY-axis
ε	process noise in pointing error
η_y	encoder initialization error (elevation)
η_z	encoder initialization error (azimuth)
θ	actual value of encoder
θ'	ideal value of encoder
ρ	slant angle of ideal and actual axes
ρ_{ryx}	rotating shaft error of elevation axis around X
ρ_{ryz}	rotating shaft error of elevation axis around Z
ρ_{rzx}	rotating shaft error of azimuth axis around X
ρ_{rzy}	rotating shaft error of azimuth axis around Y
Φ	Lagrange function